

Locomotion of Microscopic Robots in Viscous Fluids

Tad Hogg
Institute for Molecular Manufacturing
Palo Alto, CA

June 19, 2022

Abstract

Microscopic robots could perform tasks with high spatial precision, such as acting in biological tissues on the scale of individual cells, provided they can reach precise locations. This paper evaluates the feasibility of *in vivo* locomotion for micron-size robots. Two appealing methods rely only on surface motions: steady tangential motion and small amplitude oscillations. These methods contrast with common microorganism propulsion based on flagella or cilia, which are more likely to damage nearby cells if used by robots made of stiff materials. The power available to robots, e.g., from oxygen and glucose in tissue, is sufficient to support speeds ranging from one to hundreds of microns per second, over the range of viscosities found in biological tissue. We discuss design trade-offs among propulsion method, speed, power, shear forces and robot shape, and relate those choices to robot task requirements.

Keywords: nanomedicine, nanorobot, locomotion, viscous fluid

1 Introduction

Robots with sizes comparable to bacteria (nanorobots) could be useful for a wide range of biological research and medical applications. These applications can require the robots act at locations specified to precision comparable to the size of individual cells, i.e., several microns. These locations may only be recognizable once the robot is within several microns of the site, e.g., particular receptors on cell surfaces. For such precise positioning, the robots will need to find and move to their target locations themselves. Thus autonomous locomotion is a key capability for microscopic robots, which could provide significant medical benefits [22, 26, 34, 56].

Locomotion of microscopic robots faces two major challenges. The first is identifying methods appropriate for the robots' physical environment. At these sizes, viscous forces and Brownian motion are significant [17]. Thus the physics of microfluidics [29, 32, 46, 72, 82] require different locomotion methods than larger robots [66].

The second major challenge is fabricating the propulsion components and assembling them into complete robots. Some fabrication techniques have been demonstrated for small robots in fluids. One example is propulsion by magnetic fields [1, 15], which can move microrobots containing ferromagnetic particles through blood vessels [42, 55, 61]. Other demonstrated micromachines use flagellar motors [4, 57] and cilia [86]. However, locomotion of these machines is externally controlled, e.g., via magnetic fields or changing chemicals in the machine's environment, and thus are not examples of autonomous locomotion.

Nanorobots could employ various methods for autonomous motion [23]. Microorganisms provide a variety of examples. A common method is moving extended structures, such as flagella and cilia [9, 31, 43, 48, 66, 74]. These examples and current micromachines suggest appendages, such as flagella or cilia, would be good approaches for autonomous locomotion. However, appendages present significant fabrication and operational challenges for nanorobots, especially for *in vivo* nanorobot operation in close proximity with cells and many other nanorobots over extended periods of time.

The fabrication challenges for appendages include creating the active internal structures of flagella and cilia and assembling many cilia on the robot surface. More significantly, operational challenges of appendages

for locomotion include the potential for cutting nearby cells and tangling with nearby robots. Moreover, appendages expose large surface area to the environment, which could lead to fouling or immune reaction during extended *in vivo* use. Reliably avoiding these events significantly increases the complexity of the robot controller. Moreover, if a robot needs to shut down (e.g., due to component failure), appendages could become tangled by subsequent passive motion in fluids or movement of nearby cells.

To avoid these challenges, this paper focuses on the feasibility of propulsion via motion of the robot's surface without extended appendages. While not as commonly studied as propulsion by flagella or cilia, some microorganisms move without relying on appendages [18, 20, 50]. This paper examines two such methods: steady surface motion that remains flush with the robot surface, and small-amplitude surface oscillations that produce fluid behavior similar to wave motion of cilia, but without requiring any cilia.

The next section describes locomotion requirements and prototypical scenarios for microscopic robots in biological fluids. Using these scenarios as examples, the following sections evaluate the two propulsion methods. While fabrication of the nanorobots discussed in this paper is beyond current technology, these sections also discuss implementation approaches. This allows estimating internal power dissipation, which is usually neglected in studies of microscopic locomotion. Section 5 turns to the important issue of safety for these methods. The following two sections discuss the effects of robot shape and Brownian motion on locomotion. Section 8 combines these discussions to describe design trade-offs among the propulsion methods. The final section summarizes the results and suggests directions for further study.

2 Nanorobot Locomotion

Nanorobots can perform some tasks with only a coarsely-defined location. Examples include implanted nodes for communication, navigation or computation networks [23]. Such robots could, for example, be injected into the locations and have no need to actively move. Robots could accomplish other tasks by moving passively in fluids, e.g., in the blood [22]. Either all robots can perform their task this way (e.g., respiratory cells [22]) or only a few need to reach locations of interest, which is likely when using a large number of robots (e.g., monitoring for rare chemical signatures [38]).

However, fully exploiting microscopic robots requires locomotion. In particular, robots may need to actively seek specific cells identified by on-board sensors. Micron-sized robots could also move into cells [27]. Moreover, locomotion can help multiple robots coordinate their activities. For example, aggregating robots could increase concentrations of released drugs or form larger assemblies. Alternatively, robots could actively space themselves at specific distances, e.g., to distribute drug releases uniformly over a large volume, or to improve sensing by using well-separated locations for transmission and detection of signals [23].

The remainder of this section discusses performance goals for locomotion, relevant tissue properties, and example scenarios used in this paper.

2.1 Performance measures and constraints

The performance requirements for nanorobot locomotion depend on the applications and constraints on their safe use in biological environments, leading to a variety of performance measures [9], and trade-offs among them.

The main performance criteria are speed in a given direction, and maneuverability, the ability to change direction. A related property is the maximum propulsive force, e.g., to push through regions of high resistance, or exert mechanical force on cells. The maximum force depends on the strength of robot actuators and will generally be larger than the force required to move at the nominal locomotion speed.

Self-propelled robots will not necessarily need to move over long distances. Injection or passive flow could get the robots within a few hundred microns of most cells in the body. Or the robots could be carried to the vicinity of those locations inside larger devices and then released, which is particularly relevant for tasks involving machines operating cooperatively at various size scales in the same region (e.g., individual cells and the tissues they form) [39]. In such cases, autonomous locomotion need only enable robots to move about 100 μm in at most a few minutes, corresponding to locomotion speed of about 1 $\mu\text{m}/\text{s}$. The robots must

also be able change direction to go around obstacles. For example, a cell is about $10\ \mu\text{m}$ in size, so following a cell surface requires orientation changes of about 90° after $10\ \mu\text{m}$ of movement, or about 10 seconds when moving at $1\ \mu\text{m}/\text{s}$. This corresponds to angular rotation rate of about $10^\circ/\text{s}$.

These capabilities are sufficient to get to any cell of the body within minutes. These modest speed requirements leave ample design scope for other criteria, especially conservative design choices that emphasize reliability and safety over maximizing performance. Higher speeds extend the range of applications. For instance, blood flows in small vessels at speeds up to about $1\ \text{mm}/\text{s}$ [23]. Robots able to move faster than the flow could travel upstream, e.g., to track chemical gradients extending downstream from a source on the vessel wall [35]. Tasks needing higher speed even if possibly producing minor damage to tissue, e.g., responding to acute injury [24], are beyond the scope of this paper.

The limited resources available to the robot constrain feasible locomotion performance. A major constraint is power, which nanorobots may obtain in a variety of ways [23, 70, 81]. For instance, isolated micron-size robots have access to tens to hundreds of picowatts from oxygen and glucose in tissue [23, 36]. If the available power is insufficient for steady motion, the robot could move in bursts, accumulating fuel between these bursts or multiplexing movement with other tasks such as evaluating sensor readings.

Another resource constraint is the robot's surface area. Locomotion requires exerting forces against the fluid to move the robot. In the absence of extended appendages, these forces must arise from motion of the robot surface. Propulsion components on the surface compete with other surface components, such as sensors and pumps. These other uses for the robot surface favor methods that minimize surface area devoted exclusively to propulsion.

Safe locomotion requires that the robots not significantly disturb nearby cells. Disturbance can be direct, e.g., due to collisions. The speeds considered in this paper are well below safe speed limits due to collisions with cells [23]. Another direct effect is from stiff flagella cutting cells, which the methods discussed in this paper avoid by not using extended appendages. Disturbance also arises indirectly from shear forces propagated through the fluid by the moving robot. A measure of this disturbance is the magnitude of fluid flow as a function of distance from the moving robot. Smaller values mean less shear force on nearby cells, less drag from nearby walls and less hydrodynamic interaction among nearby robots, which could simplify controls.

2.2 Thrust Force and Power Dissipation

Locomotion has two contributions to power dissipation. First is the power, P_{propel} , dissipated through viscosity in the fluid. Second is the dissipation, P_{internal} , within the robot to actuate the propulsion components. The sum $P_{\text{propel}} + P_{\text{internal}}$ gives the power directly required for locomotion. Additional losses within the robot, such as for the computer to control robot motion or to generate and distribute power [23] are not considered here.

External power use arises from the fluid flow around the moving object. A simple case is an externally forced spherical robot. The force required to drag a sphere of radius a at speed U through an unbounded fluid of viscosity η is given by Stoke's law

$$F = 6\pi\eta aU \quad (1)$$

when the Reynolds number, $aU\rho/\eta$, is small, where ρ is the density of the fluid. The power dissipated in the fluid is $P_{\text{drag}} = FU$. Conversely, for an arbitrary propulsion mechanism that moves the sphere at speed U , applying an external force F to the robot against the direction of the motion will stop the robot. Thus Eq. 1 estimates the thrust force of a propulsion mechanism capable of moving at speed U .

A common measure of locomotion effectiveness is its *hydrodynamic efficiency* [48,53]: the ratio $P_{\text{drag}}/P_{\text{propel}}$ of the power required for an external force to drag the object through the fluid to the power required for the object to propel itself at the same speed. Hydrodynamic efficiency is typically a few percent [66].

Studies of microorganism locomotion typically focus entirely on hydrodynamic efficiency, which only accounts for energy dissipated in the fluid. A full evaluation of power use must also account for power dissipated inside the robot. This is particularly important for situations with large hydrodynamic efficiency [50,71] where P_{propel} is very small so power use is dominated by internal dissipation. Even for less efficient loco-

motion, estimates of microorganism propulsion by cilia suggest dissipation required to move the cilia is comparable to or larger than dissipation in the fluid motion around the organism induced by the cilia motion [45].

Internal dissipation depends on the details of the actuator mechanisms which, in general, are not known well enough to allow useful power estimates for either microorganisms or micromachines. For instance, a variety of effects contribute to friction in micromachines [47, 78], depending on the microstructure of the surfaces, lubrication, applied forces and operating speeds. However, nanorobots made of precisely structured, stiff materials, could be much more efficient [14] than currently demonstrated micromachines, in part due to avoiding viscous losses inside the robot by excluding fluid from the interior. In this case, internal dissipation is primarily due to friction between moving actuators and their housings in the robot. Smooth nanoscale surfaces separated by atomic-scale distances (i.e., a few tenths of a nanometer) moving past each other at speed v well below that of sound in the material have friction dominated by phonon scattering [14]. This leads to power loss

$$P_{\text{friction}} = k_{\text{friction}} S v^2 \quad (2)$$

where S is the area of the moving surfaces and k_{friction} is a constant depending on the materials and their spacing. For stiff materials, k_{friction} is generally less than $1000 \text{ kg}/(\text{m}^2\text{s})$ [14, 23]. We use this value to give an upper bound estimate for internal power loss, i.e., taking $P_{\text{internal}} \approx P_{\text{friction}}$. Thus, unlike the complexity of friction in micromachines with poorly defined geometry at nanometer scales, friction dissipation in smooth nanoscale surfaces has a simple dependence on area and speed. This allows estimating internal power dissipation for the implementations considered in this paper more readily than is possible for current micromachines.

For comparison, the viscous friction for flat surfaces moving past each other at speed v while separated by a layer of fluid with viscosity η and thickness d is $\eta S v/d$. This dissipates power $(\eta/d) S v^2$, so $k_{\text{friction}} = \eta/d$. Extrapolating to distances of a few tenths of a nanometer gives $k_{\text{friction}} \approx 10^7 \text{ kg}/(\text{m}^2\text{s})$ for fluids with viscosity similar to water. Similarly, measurements of drag for micromachine rotors [10] gives k_{friction} of about this size. More precisely defined micron-scale surfaces can have lower friction [84], but still significantly larger than the value of k_{friction} given above. Thus the internal dissipation we consider for nanorobots, while achievable in principle, is several orders of magnitude smaller than that of current micromachines. This lower friction is important in the feasibility of the propulsion mechanisms considered here, which would otherwise require more power than available to nanorobots. By contrast, the large friction of current micromachine components requires much higher power (e.g., via external forces that move the robot) or propulsion mechanisms with fewer moving parts, such as rigid, extended appendages.

2.3 Scenarios

Fluid density and viscosity determine the nature of locomotion. In biological tissues, viscosity varies by orders of magnitude while density is roughly the same. Thus as scenarios illustrating behaviors in biological tissue, we consider a wide range of viscosity but with constant density. For the short distances we consider ($\sim 100 \mu\text{m}$, about 5 to 10 cell diameters), we assume a homogeneous fluid.

Specifically, these scenarios are moving in 1) a low viscosity fluid (comparable to water) at about $100 \mu\text{m}/\text{s}$, and 2) a high viscosity fluid 10^4 times more viscous than water, which is a typical value for mucus or cell cytoplasm [23]. Power use is proportional to the product of viscosity and the square of locomotion speed, so we consider a speed of $1 \mu\text{m}/\text{s}$ in the high viscosity case to give the same power requirements for both scenarios.

Medical nanorobots could vary in size, from about one to tens of microns. Mobile robots able to access individual cells will generally be small, e.g., to allow passing through the smallest blood vessels and between or into cells. We focus on such sizes, i.e., robots that are a few microns in size. Robot shape also influences locomotion behavior. We mainly focus on spherical robots for simplicity.

Table 1 gives the fluid and robot parameters for these scenarios. In both cases, the Reynolds number is much less than one, indicating viscous forces dominate the fluid behavior [66].

scenario		both	LOW	HIGH
speed of sound	c	1500 m/s		
density	ρ	1000 kg/m ³		
ambient temperature	T_{body}	310 K		
viscosity	η		10^{-3} Pa · s	10 Pa · s
kinematic viscosity	$\nu = \eta/\rho$		10^{-6} m ² /s	10^{-2} m ² /s
radius of spherical robot	a	1 μm		
locomotion speed	U		100 $\mu\text{m/s}$	1 $\mu\text{m/s}$
Reynolds number	aU/ν		10^{-4}	10^{-10}
force	$F = 6\pi\eta aU$		2 pN	200 pN
power to drag	$P_{\text{drag}} = FU$		2×10^{-4} pW	2×10^{-4} pW

Table 1: Scenarios corresponding to motion in low and high viscosity biological fluids. The LOW scenario corresponds to water and the HIGH scenario to fluids 10^4 times more viscous than water. Values in the third column apply to both scenarios.

3 Propulsion by Steady Tangential Surface Motion

Steady tangential movement of the robot surface involves motion whose speed is constant in time but may vary at different locations on the surface. For instance, Fig. 1a illustrates axially symmetric surface motion on a sphere where material moves from north to south pole, expanding and contracting as it moves. Material accumulating at the south pole is recycled within the robot to reappear at the north pole.

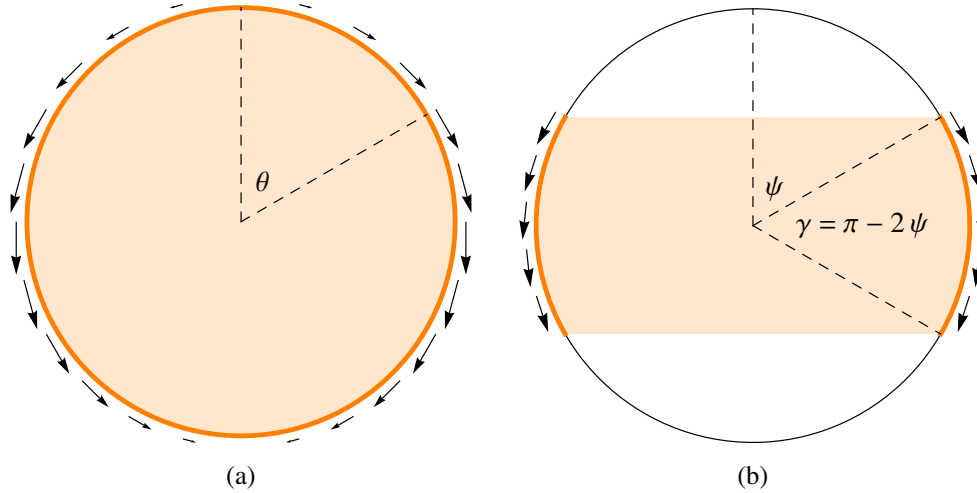


Figure 1: Tangential motion, indicated by arrows, on a cross section of a sphere. In this case, motion is axially symmetric. The shaded areas indicate the extent of the motion. Points travel inside the robot to return to their original locations (not shown). (a) Speed at polar angle θ proportional to $\sin \theta$. (b) Constant speed in a band, of angular size γ , around the equator, consisting of θ in the range $\psi \leq \theta \leq \pi - \psi$ where $\psi = (\pi - \gamma)/2$, and no propulsion on the rest of the surface.

A robot needs some surface area for other components, such as sensors and pumps. Embedding them in a surface moving inside the robot significantly increases the difficulty of fabricating the components, including their connection to other parts of the robot. Thus practical propulsion with this surface motion uses only part of the surface, in contrast with studies allowing motion on the full surface [50, 59, 64]. Fig. 1b shows such an approach: the surface only moves within a band of angle γ centered on the equator, and, for simplicity, the motion is with constant velocity.

scenario		LOW	HIGH
propulsion band angle	γ	60°	60°
surface area fraction	$\sin(\gamma/2)$	1/2	1/2
surface speed	v	210 $\mu\text{m/s}$	2.1 $\mu\text{m/s}$
locomotion speed	$U = \frac{1}{4}v(\gamma + \sin(\gamma))$	100 $\mu\text{m/s}$	1 $\mu\text{m/s}$
power	$8\pi a\eta v^2 \sin(\gamma/2)$	0.00055 pW	0.00055 pW
hydrodynamic efficiency	$\frac{3}{64}(\gamma + \sin(\gamma))^2 \csc(\gamma/2)$	0.34	0.34
max. thrust	$6\pi a\eta U$	1.9 pN	190 pN

Table 2: Performance of tangential motion in an equatorial band on a sphere, illustrated in Fig. 1b, computed from Eq. 3 and 5 using parameters of Table 1.

propulsion band angle	γ	60°
surface area fraction	$\sin(\gamma/2)$	1/2
max. surface speed	v	100 $\mu\text{m/s}$
angular velocity	$\Omega = 2\frac{v}{a} \sin(\gamma/2)$	100 rad/s

Table 3: Example performance for rotation via tangential motion on a sphere with radius $a = 1 \mu\text{m}$.

3.1 Performance

For simplicity in quantifying the performance of steady surface motion, we focus on spherical robots. This analysis applies to motion at low Reynolds number and generalizes to spheroids [50]. For a sphere with radius a , tangential surface motion $u(\theta, \phi)$ at the point specified by spherical coordinates θ, ϕ gives locomotion velocity U and angular velocity Ω [73]

$$U = -\frac{1}{4\pi a^2} \int_S u \, dS \quad (3)$$

$$\Omega = -\frac{3}{8\pi a^3} \int_S n \times u \, dS \quad (4)$$

where n is the unit outward normal vector to the sphere surface S . For axisymmetric surface motion, i.e., $u(\theta, \phi)$ independent of azimuthal angle ϕ , the sphere does not rotate, i.e., $\Omega = 0$, and the power required to produce this locomotion is [73]

$$P_{\text{propel}} = \frac{2\eta}{a} \int_S |u|^2 \, dS \quad (5)$$

The velocity distribution $u(\theta) = v \sin(\theta)$ gives the maximum hydrodynamic efficiency, of 50%, for a sphere [50, 64]. In this expression, v is the maximum surface speed and $U = \frac{2}{3}v$ from Eq. 3. Tangential motion using only part of the surface, as shown in Fig. 1b, is only somewhat less efficient, as shown in Table 2.

For a robust design, the surface speed v will be well within the strength limits of the robot's actuators. Thus the maximum surface speed the actuators can produce, and hence thrust available to the robot, as determined by the strength of the surface material and motors internal to the robot, could be considerably larger than the values indicated in the table.

Rotating the robot requires non-axially symmetric surface motions. An example is the surface motion $u(\theta, \phi) = v \cos(\phi)$ on an equatorial band of angle γ , shown in Fig. 2. In this case, Eq. 4 gives the angular velocity shown in Table 3, which is oriented along the negative y-axis. The time required to change orientation of the sphere by angle α is $t = \alpha/\Omega$. If the actuators can move in both directions through the equatorial band, there is no need to rotate the robot to move in the opposite direction. In that case, the largest required rotation is 90°, requiring time $t = \pi/(2\Omega)$. For the example in Table 3, this rotation takes about 15 ms. By comparison, a robot moving at 100 $\mu\text{m/s}$ travels a distance of a cell diameter in about 100 ms, so this rotation rate readily allows adjusting direction without significantly affecting the time required for the motion around cells.

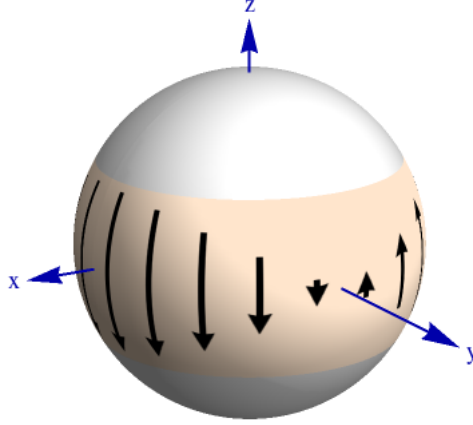


Figure 2: Surface motion $u(\theta, \phi) = v \cos(\phi)$ on an equatorial band that rotates the sphere around the y -axis. Arrows indicate the direction of surface motion, with lengths proportional to the speed.

3.2 Implementation

Two implementations that approximate steady tangential motions are treadmills and small wheels on the surface. These do not produce exactly tangential motion, e.g., where the tread penetrates the robot surface, nor precisely the expressions for the surface speed, $u(\theta, \phi)$, discussed above, e.g., due to gaps between wheels. Nevertheless, they approximate tangential surface motions discussed above, thereby approximately implementing the locomotion performance described above.

In the implementation considered here, all the components move in the same direction, aligned with one axis of the sphere. This matches the surface motions discussed above and is sufficient for general locomotion as a combination of motion in the direction of that axis and rotating the robot to orient that axis in arbitrary directions.

3.2.1 Treadmills

Fig. 3 shows treadmills on an equatorial band, corresponding to the parameters of Table 2, i.e., propulsion using half the sphere's surface area. In this diagram, the tread runs over the outer surface, thereby producing motion of a spherical surface evaluated here¹. The figure shows gaps between treads. The performance analysis given above corresponds to narrow gaps between treadmills, so the treadmills cover most of the surface of the equatorial band.

To evaluate structural requirements for a treadmill, consider a tread of length L , width W , area $A = LW$ and thickness h pulled at speed v around bearings of radius r . The bearings turn at angular frequency $\omega = v/r$. To estimate of the force applied to the fluid, consider a treadmill moving a distance d from a wall (where fluid speed is zero). The force on the tread area exposed to the fluid is $F = \eta \nabla v A$ with velocity gradient is $\nabla v \approx v/d$. This force stretches the tread, resulting in strain $(F/(Wh))/E$ where Wh is the tread's cross section area and E is Young's modulus of the material. For bending the tread around the bearings, the distance of the tread along inner and outer edges is πr and $\pi(r+h)$, respectively, giving strain of $h/(r+h/2) \approx h/r$ for $h \ll r$ and corresponding stress of Eh/r .

The tread tension due to fluid drag in Table 4 is far below the failure strength, typically at least 10^{10} Pa, of strong materials. So such treadmills can readily provide forces that produce the speeds considered here, even in fluids with several orders of magnitude higher viscosity. The tread has substantial strain as it bends around the bearing. If necessary to reduce this strain, the bearing radius could be somewhat larger, thereby requiring

¹An alternate implementation has the tread running straight between the two bearings, corresponding to a robot shaped as a cylinder with spherical caps at each end.

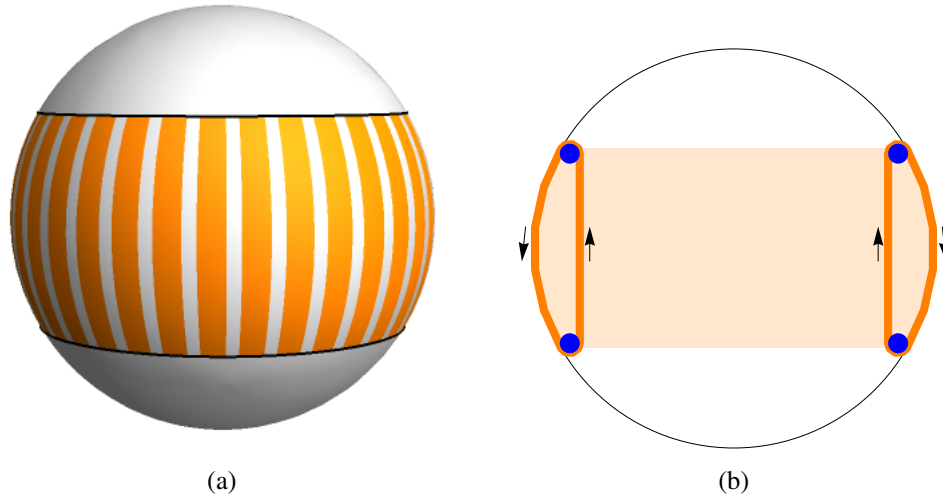


Figure 3: (a) Schematic of a set of treadmills on a band around the equator of a sphere. Treads move vertically, from top to bottom of the band and are separated by narrow gaps. (b) Cross section showing internal movement of treadmills. Blue disks indicate the bearings, and arrows indicate motion of the treadmills when they all move in the same direction, giving axially symmetric motion.

	tread	
width	W	100 nm
length exposed to fluid	L	$1 \mu\text{m}$
thickness	h	1 nm
Young's modulus	E	1000 GPa
tread speed	v	$210 \mu\text{m/s}$
	bearing	
radius	r	50 nm
rotation rate	$f = v/(2\pi r)$	0.7 kHz
angular velocity	$\omega = v/r$	4200 rad/s
	tread bent around bearing	
strain	h/r	2%
stress	hE/r	20 GPa
	forces when moving $d = 100 \text{ nm}$ from a wall	
drag on tread from fluid	$F = \eta(v/d)LW$	0.2 pN
tension on tread cross section	$F/(hW)$	2000 Pa

Table 4: Example parameters for treadmill. Tread speed corresponds to the LOW scenario of Table 2.

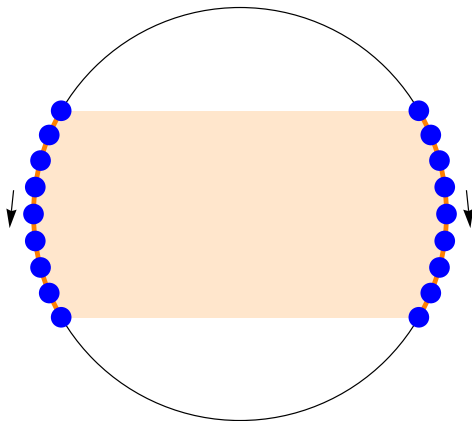


Figure 4: Schematic wheel propulsion in a band around the equator. Blue disks indicate the wheels, and arrows indicate motion when the wheels all move in the same direction, giving axially symmetric motion. In this case, wheels on the left (right) rotate counterclockwise (clockwise).

more of the robot’s interior volume for propulsion components. Alternatively, the tread could be thinner. An extreme limit for a thin tread is a single-atom layer, e.g., graphene with elastic modulus $E = 10^{12}$ Pa, and breaking strength around 10^{11} Pa [49] In summary, Table 4 shows an implementation of tangential motion using treadmills is feasible with the mechanical properties of strong materials.

3.2.2 Wheels

The speed along a treadmill is constant, so treadmills extending the full width of the equatorial band (as illustrated in Fig. 3) have speed on the band, $u(\theta, \phi)$, that does not vary with the polar angle θ . This is suitable for the constant speed discussed in Table 2, but not for motions such as illustrated in Fig. 1a. Using a series of shorter treadmills could approximate such motions, and give somewhat higher efficiencies. An extension of this idea is to forego the tread and instead use a set of closely-spaced wheels. If the wheels have small diameter compared to the size of the robot, their motion approximates the tangential surface motion discussed above². Fig. 4 illustrates this implementation.

The stress on the wheels due to their rotation is negligible compared to their strength. Specifically, the stress on a disk of density ρ and radius r rotating with angular velocity ω is $\sim \rho v^2$ where $v = r\omega$ is the velocity of the outer edge [23]. As an example, wheels similar to the bearings of Table 4 have $r = 50$ nm, $v \sim 200 \mu\text{m/s}$, and density of $\sim 5000 \text{ kg/m}^3$. This gives stress $\rho v^2 \approx 10^{-4}$ Pa, far below the material strength.

3.2.3 Comparing treadmills and wheels

Both treadmill and wheel implementations can approximately produce tangential surface motion.

Compared to wheels, treadmills have fewer bearings (hence fewer internal components connecting bearings to motors), and fewer breaks in the robot surface. Each break in the surface has the potential to leak fluid into the robot, so minimizing such breaks could increase locomotion reliability. Moreover, treadmills approximate tangential surface motion more accurately than wheels. In particular, the narrow gaps between adjacent wheels along a meridian of longitude will have large fluid shear where the wheels’ edges enter and exit the robot. Moreover, some area on the sides of the wheels extends into the fluid, producing additional drag. Thus wheels will produce more fluid dissipation than treadmills, especially at higher speeds, e.g., for the LOW scenario.

²This contrasts with propulsion by a few larger thin wheels [23] which extend a significant distance from the robot surface and hence could cut into nearby cells.

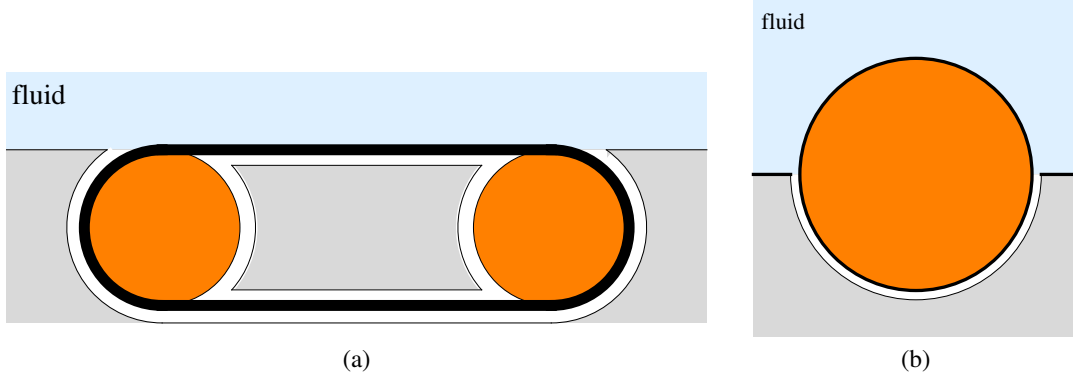


Figure 5: (a) Schematic treadmill and bearings sliding in a housing (gray). The bearing and gap sizes are exaggerated relative to length of the tread. (b) Schematic wheel positioned halfway inside the robot (gray). The gap size is exaggerated relative to wheel. In both cases, the rotating parts also slide against robot housing on either side, into and out of the page (not shown), which separates these components from those at neighboring meridians of longitude on the robot surface.

On the other hand, wheels can produce a wider range of surface motions since the wheels along a longitude meridian need not move at the same rate or same direction. For example, varying the wheel speed as a function of latitude can improve hydrodynamic efficiency compared to constant speed vs. latitude of treadmills. Moreover, force sensors associated with each wheel give more spatial resolution about the robot surface than the force on a tread, thereby enabling higher resolution feedback control.

3.2.4 Internal power dissipation

Treadmills and wheels have about the same area of internal sliding surfaces, giving comparable power loss due to internal motion. For the tread parameters of Table 4, about 50 treadmills cover the equatorial band of the sphere (Fig. 3a) with total sliding area of about $20 \mu\text{m}^2$ for all the treads and their bearings (Fig. 5a). With this sliding surface area and the tread speeds matching the surface speeds in Table 2, Eq. 2 gives P_{friction} of 10^{-3} pW and 10^{-8} pW for the LOW and HIGH scenarios, respectively. Comparing to Table 2, these estimates suggest internal power dissipation is a bit larger than the external loss for the LOW scenario, similar to the situation for microorganisms using cilia [45]. On the other hand, P_{friction} is much lower than external loss for the HIGH scenario, so the high viscosity of the fluid dominates the total power use.

For wheels using the same width and radius as for the treadmill bearings of of Table 4, about 500 wheels cover the equatorial band on the sphere, with surface area comparable to that of the treadmill internal surfaces. The position of the wheel center relative to the robot surface is a design choice. For example, with the center at the robot surface (Fig. 5b), half of each wheel’s circumference slides against the robot housing, giving P_{friction} of 5×10^{-4} pW and 5×10^{-9} pW for the LOW and HIGH scenarios, respectively. If wheel centers are positioned a bit below the robot surface, more of their surface will slide against the robot housing, the smaller portion in the fluid will more closely approximate tangential motion, and there will be larger gaps between the portions of neighboring wheels that move next to fluid. With the approximate nature of these estimates for internal power dissipation, these values indicate treadmills and wheels have similar internal dissipation.

4 Propulsion by Surface Oscillations

Periodic surface oscillations can propel a robot via traveling surface waves [8]. These waves can travel over the full extent of the surface, e.g., from north to south pole on a sphere, even though individual points on the surface move only a small distance.

To specify the oscillation, we label points on the surface by their location on the undistorted sphere. For axially symmetric motion, all points with the same polar angle move the same way, so a point’s polar angle

on the undistorted sphere, ϑ , completely determines its motion. Fig. 6 illustrates this notation. The position of the point at time t can be expressed as a sum over oscillation modes:

$$r = a \left(1 + \epsilon \sum_{n=2}^{\infty} \alpha_n(t) P_n(\cos \vartheta) \right) \quad (6)$$

$$\theta = \vartheta + \epsilon \sum_{n=2}^{\infty} \beta_n(t) V_n(\cos \vartheta) \quad (7)$$

where amplitudes α_n and β_n are periodic functions with period $T = 2\pi/\omega$, ω is the angular oscillation frequency, $P_n(x)$ is the n^{th} Legendre polynomial and

$$V_n(x) = \frac{1}{n+1} P_n^1(x) \quad (8)$$

where P_n^1 is the associated Legendre polynomial of order 1 [62]. Modes with large n correspond to surface oscillations with short wavelengths.

We define the amplitudes at time t as

$$\begin{aligned} \alpha_n(t) &= \Re(e^{-i\tau+i\gamma_n}) A_n \\ \beta_n(t) &= \Re(e^{-i\tau+i\eta_n}) B_n \end{aligned} \quad (9)$$

where $\Re(z)$ is the real part of the complex number z , $\tau = \omega t$, A_n and B_n are nonnegative, and the angles γ_n and η_n specify the phases of the radial and tangential components of the motion, respectively.

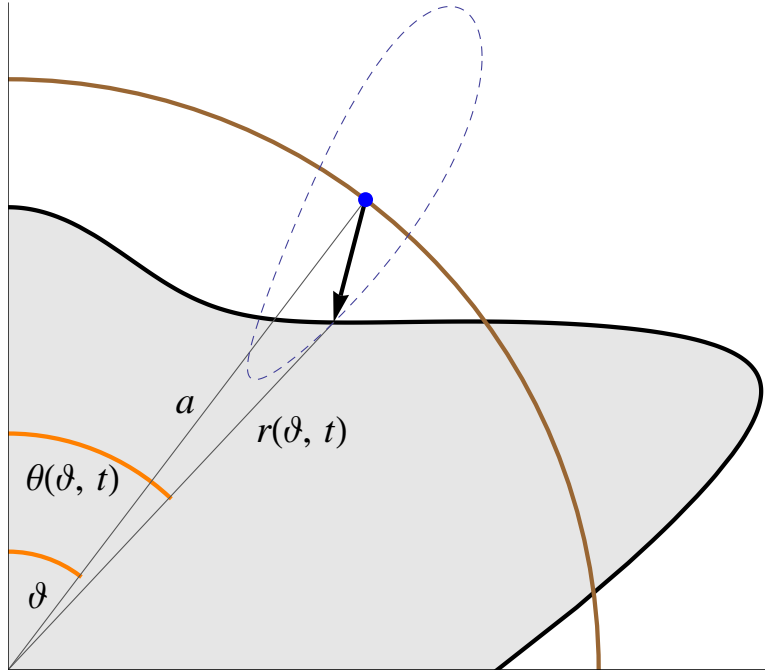


Figure 6: Notation for axially symmetric distorted sphere, showing a cross section of a portion of the distorted sphere (gray) and undistorted surface (brown circle). At time t , the material point at radius a and angle ϑ on the undistorted sphere is displaced as indicated by the arrow to location r, θ . During an oscillation period, the material point moves around the dashed curve. The cases we consider have maximum distortion of a few percent of the radius a , so the distortion in this figure is exaggerated.

For simplicity, we focus on small amplitude surface oscillations. Such oscillations are convenient for two reasons. First, piezoelectric materials can implement such oscillations. Second, small amplitude oscillations

scenario		LOW	HIGH
oscillation frequency	f	2 kHz	0.02 kHz
angular frequency	$\omega = 2\pi f$	1.3×10^4 rad/s	1.3×10^2 rad/s
viscous damping length	$\delta = \sqrt{2\nu/\omega}$	13 μm	13000 μm
Womersley number	$a\sqrt{\omega/\nu}$	0.1	10^{-4}

Table 5: Oscillation frequency and criteria for quasi-static Stokes fluid flow using parameters of Table 1.

of simple geometries, such as a sphere, are analytically-tractable [6, 32]. Neither of these reasons is necessary: metamorphic surfaces can give large shape changes [23], and numerical methods [59] can evaluate locomotion for large amplitude deformations [68].

4.1 Performance

Determining locomotion performance from oscillating surfaces requires evaluating the fluid flow around the robot. We focus on axially symmetric oscillations, which simplifies the analysis and gives the highest hydrodynamic efficiency [69]. Due to viscous damping, fluid motion a distance d from the surface is proportional to $e^{-d/\delta}$ where $\delta = \sqrt{2\nu/\omega}$ is the viscous damping length and $\nu = \eta/\rho$ is the kinematic viscosity [21]. When this damping length is large compared to the size of the robot, i.e., when $a/\delta \ll 1$, the flow is quasi-static: fluid response to each position of the oscillating robot is approximately the same as fluid would respond if the geometry were frozen in that configuration with boundary conditions determined by the shape and velocity of the surface at that time [46]. Corrections to the quasi-static approximation are of order $a\sqrt{\omega/\nu}$, the Womersley number [46]. This approximation treats the fluid as incompressible, which requires that motions are slow compared to the speed of sound, i.e., $a\epsilon\omega \ll c$, which holds for the scenarios considered here.

For small distortions (i.e., $\epsilon \ll 1$), the fluid velocity and pressure around the sphere are proportional to $\epsilon\omega$, locomotion speed is proportional to $\epsilon^2\omega$ and power is proportional to $\epsilon^2\omega^2$ [6, 69]. Comparing the scenarios of Table 1 involves choices of oscillation amplitude and frequency, i.e., values for ϵ and ω . The scenarios specify locomotion speed, which constrains the product $\epsilon\omega$ but not the individual values. As a specific choice, we consider the same oscillation amplitude, i.e., the same value of ϵ , in both scenarios and vary the oscillation frequency to give the specified locomotion speeds. Table 5 gives these parameters for both scenarios, and shows the quasi-static approximation is reasonable.

The remaining design question is the shape of the oscillations, i.e., choices for the magnitude and phase of the amplitude for each mode, given in Eq. 9. Maximum hydrodynamic efficiency occurs in the limit of a large number of infinitesimally small wavelengths [69]. However, there is only minor increase in efficiency when using wavelengths smaller than about 1/10 the robot size, corresponding to modes with $n \approx 10$. Moreover, high modes have significantly different motions of nearby points on the surface, which require more precise control, and possibly more internal power dissipation in the actuators. Thus practical propulsion with surface oscillations will not use the arbitrarily large modes that maximize hydrodynamic efficiency.

The optimal amplitudes have a simple form in the limit of large modes [69] and are close to optimum when applied to a finite set of modes $n = k, \dots, k + p$. Specifically, these choices for the amplitudes in Eq. 9 are

$$A_n = (1 + \sqrt{2}) \sin(j\psi) \quad (10)$$

$$B_n = \sin(j\psi) \quad (11)$$

$$\gamma_n = -\frac{\pi}{2}(j - 1) \quad (12)$$

$$\eta_n = -\frac{\pi}{2}(j - 1) \quad (13)$$

with $j = n - k + 1$, $\psi = \pi/(p + 2)$, and otherwise $A_n = B_n = 0$. The amplitudes multiply ϵ to produce the distortion of Eq. 6, so have an arbitrary overall scale. We fix this scale by normalizing amplitudes so the largest displacement of any point on the sphere over the entire oscillation period is $a\epsilon$.

As an illustration, Fig. 7 shows the surface distortions for $k = 10$, $p = 10$. The oscillations form waves

scenario		LOW	HIGH
max. surface displacement	$a\epsilon$	$0.05 \mu\text{m}$	$0.05 \mu\text{m}$
max. surface speed	$a\epsilon\omega$	$620 \mu\text{m/s}$	$6 \mu\text{m/s}$
locomotion speed	$3.29 a\epsilon^2\omega$	$100 \mu\text{m/s}$	$1 \mu\text{m/s}$
power	$65.5 a^3\epsilon^2\eta\omega^2$	0.025pW	0.025pW
hydrodynamic efficiency	$3.12 \epsilon^2$	0.008	0.008
max. thrust	$62.1 a^2\epsilon^2\eta\omega$	1.9pN	190pN

Table 6: Performance of oscillating sphere using parameters of Tables 1 and 5, $\epsilon = 0.05$ and amplitudes of Eq. 10 for $n = k, \dots, k + p$, with $k = p = 10$, normalized so maximum surface displacement is $a\epsilon$. The second column shows how the measures depend on geometry, oscillation amplitude and frequency, and fluid viscosity [6].

traveling from the north to south pole, with the largest surface motions close to the equator. Table 6 shows the performance of this locomotion. Even though hydrodynamic efficiency is low, the total power required is well below that likely available to such robots.

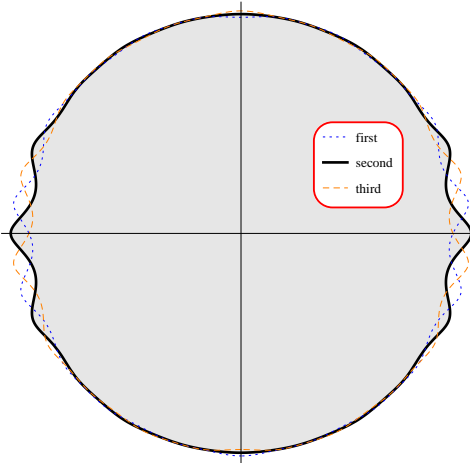


Figure 7: Cross section of oscillating sphere at three equally spaced times during an oscillation period, in the order dotted (first), solid (second) and dashed (third). The gray region corresponds to the second position shown. Waves of surface distortion move from top to bottom, which is opposite the locomotion direction.

Fig. 8 shows the behavior of the fluid near the oscillating surface [6]. The magnitudes of the fluid velocity and pressure variation decrease rapidly away from the oscillating surface.

4.2 Implementation

Microorganisms that move via coordinated waves of moving cilia produce fluid motion similar to small amplitude oscillations of the virtual surface formed by the outer envelope of those cilia [9]. Similarly, robots could use many closely-spaced short appendages to produce surface waves. However, using cilia reduces surface available for other devices, and cilia expose more surface area to the fluid which may be more likely to provoke immune reactions. Instead, we consider two direct implementations of surface oscillations: electrically actuated piezoelectric materials and rods actuated by motors under a flexible surface. This contrasts with treadmill or wheel-based locomotion that use devices embedded in the surface that directly drag against the fluid. Thus, surface oscillations have the advantage of not requiring propulsion components on the surface itself, thereby leaving the surface available for other devices, e.g., sensors, provided they are flexible enough to function in spite of distortions.

Alternatively, a mixed implementation could be useful with the piezoelectric material providing fine scale adjustments while portions of the surface requiring large oscillations (i.e., near the equator) use motors to

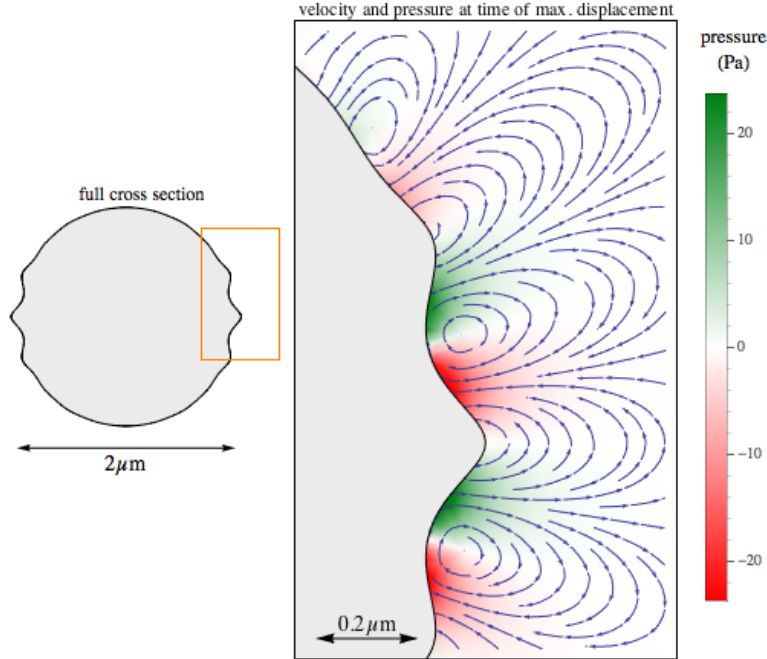


Figure 8: Velocity streamlines and pressure in fluid around an oscillating sphere at the time during an oscillation period of maximum displacement for the LOW scenario. The parts of the surface with positive pressure, indicated in green, are moving outward, while parts with negative pressure are moving inward. The rectangular box on the full cross section at the left corresponds to the region shown in detail on the right.

produce most of the distortion.

4.2.1 Piezoelectric actuators

Piezoelectric materials change size in response to electric fields, with the change in length per volt of potential difference ranging up to $d = 0.5 \text{ nm/V}$ or so [77]. Piezoelectrics usually involve tiny motions, but some can produce strains of up to 5% [85], as used in the example of Fig. 7. These materials are typically ceramics, although piezoelectric behavior also occurs in thin sheets such as graphene [63]. The pressures on the robot from the fluid will have negligible effect on these materials. Specifically, piezoelectric materials have Young's modulus of $E \sim 10^{10} \text{ Pa}$ or more. Thus typical pressure changes in the fluid due to oscillations (e.g., tens of pascals, shown in Fig. 8) give negligible changes in size.

The maximum displacement in the example of Fig. 7 is $a\epsilon = 50 \text{ nm}$, near the equator. Such displacements would require $a\epsilon/d \approx 100 \text{ V}$ across the material. Applied across an equatorial slab of material within a robot with $1 \mu\text{m}$ radius, this corresponds to an electric field of 10^8 V/m , at the upper end of fields encountered in microscopic biological contexts [23], though in this case the field is internal to the robot. Such fields are considerably larger than usually applied to piezoelectrics, and thus may damage the material, e.g., by altering the polarization that gives rise to the piezoelectric effect. Another difficulty in using piezoelectrics for the oscillation sizes considered here is their power dissipation, with dielectric losses typically 1% of the energy involved in storing charge on the material [58].

Thus, unless significantly more responsive (i.e., larger d values), robust and low-dissipation piezoelectric materials become available, their use will be limited to smaller oscillations (i.e., smaller ϵ) than the example in Fig. 7. This would give slower locomotion. Alternatively, using higher oscillation frequencies would achieve the same locomotion speed, but such combinations of smaller ϵ and larger ω would dissipate more power in the fluid, as shown in Table 6.

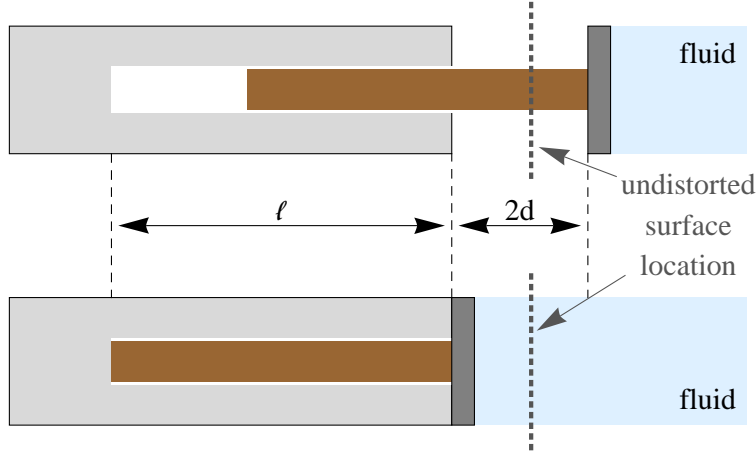


Figure 9: Schematic of a rod moving a portion of the robot surface at the times of the oscillation period with maximum (top) and minimum (bottom) displacement. The motion range is twice the maximum displacement d from the undistorted location (thick dotted line). The size of the gap between the rod and its housing is exaggerated. The segment of surface pushed by the rod is shown as a straight segment, but will actually bend to join with surface segments displaced differing distances by neighboring rods.

4.2.2 Oscillating rods

Mechanical forces on a deformable surface can produce surface oscillations. A direct approach to creating such forces is to use motors to independently push on different parts of the surface. For example, Fig. 9 shows a rod displacing a portion of the surface at two different times, corresponding to maximum and minimum of the surface distance from the center of the robot. Motors [14] could periodically move the rods to produce desired oscillations patterns.

The rods indicated in the figure actuate the surface in one direction, i.e., radially, so any tangential motion would be a side effect of stretching the surface due to neighboring rods. A more complex rotary mechanism would be needed to produce a specific combination of radial and tangential motion illustrated in Fig. 6. Alternatively, restricting oscillations to purely radial surface motion reduces locomotion speed compared to the optimal motions, which have both radial and tangential motions of Eq. 10. For example, with no tangential motion (i.e., $B_n = 0$), the locomotion speed is 60% of the value in Table 6.

To produce the traveling waves on the surface, actuators must be able to independently move regions of the surface corresponding to the highest modes with nonzero amplitude. The example of Table 6 uses modes up to $k + p = 20$. This requires independent motions at distances of $\delta = \pi a/20 \approx 150$ nm, and hence about $4\pi a^2/\delta^2 \approx 500$ rods actuating the surface.

The main displacement is near the equator, leading to two implementation approaches. First, the robot could have rods uniformly spread across the surface. This would allow the robot to change direction by simply altering the oscillation pattern of the rods to correspond to the north-to-south axis oriented in the new direction. Second, the robot could have actuators only in a band around its equator, thereby ignoring the small oscillations outside that band indicated by the amplitudes of Eq. 10. Such an implementation would use fewer rods than the full implementation, but would need to rotate the robot to new directions, using non-axisymmetric oscillations analogous to those illustrated in Fig. 2 for tangential motion.

As an example to estimate internal power use, consider 500 rods each with radius $r = 50$ nm and length $\ell = 5d$, or 250 nm. and the full circumferential area $S = 2\pi rL$ sliding past the rod housing throughout the oscillation, i.e., we count the portion of the rod sticking out of the housing as also contributing to sliding friction. This gives about $S = 40 \mu\text{m}^2$ as the combined sliding surface area for all the rods.

The speed of the surface, and hence the rods, oscillates. Averaging Eq. 2 over an oscillation period $2\pi/\omega$ gives $P_{\text{friction}} = (1/2)kSv^2$ where v is the maximum speed of the rod during the oscillation. As

a simple upper bound on the internal dissipation, we consider all the rods oscillating with this maximum displacement, so v is the maximum surface speed $a\omega\epsilon$, given in Table 6. These choices give P_{friction} less than 8×10^{-3} pW and 8×10^{-7} pW for the LOW and HIGH scenarios, respectively. These values are smaller than the external power dissipation for both scenarios (Table 6), indicating internal dissipation is not significant for this implementation. Nevertheless, these values for P_{friction} are larger than for tangential motion discussed in Section 3.2.

5 Effects of Locomotion on Nearby Cells and Robots

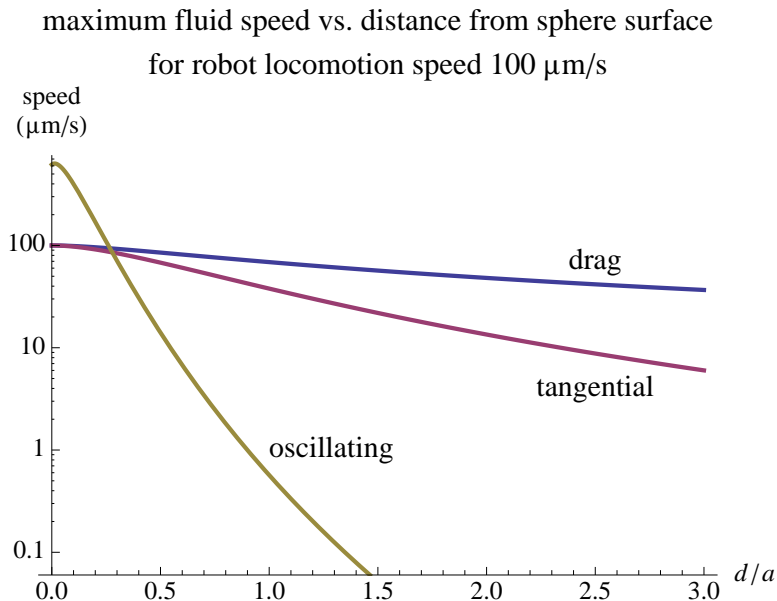


Figure 10: Maximum fluid speed due to a spherical robot, with $1 \mu\text{m}$ radius, vs. distance d from robot surface, relative to robot radius a , for different modes of locomotion in the LOW scenario.

Fluid motion can affect cells [12, 13, 25, 65, 79] including changes in gene expression [11]. A minimal disturbance is the change in flow that activates mechanical sensors on the cell. For example, some cells can detect changes in velocity as little as $20 \mu\text{m/s}$, shear (spatial gradients of velocity) in the range $1\text{--}10/\text{s}$ [31], and fluid stress as low as 1 Pa [40].

Such biological responses suggest conservative limits for microscopic robot locomotion are forces up to 10 pN and shear stresses up to $1\text{--}100 \text{ Pa}$ [25]. This range of stress is well below that required to significantly distort or rupture cell membranes [23, 60]. The viscous stress from the fluid is $\eta\nabla v$. For the LOW scenario of Table 1, a shear of $1000/\text{s}$ gives a stress of 1 Pa .

As an indication of the relative safety, Fig. 10 illustrates maximum fluid speed produced by the moving robot for three locomotion methods: dragging by an external force, and the two methods discussed in this paper: steady tangential surface motion and small oscillations. Self-propelled robots disturb the fluid less than a robot dragged by an external force, which is also the case for microorganism movement [45].

A change in velocity of at least $20 \mu\text{m/s}$ occurs only within less than a micron from a sphere using tangential propulsion to move at $100 \mu\text{m/s}$, but several microns for a sphere dragged by an external force. Using surface oscillations has larger effects close to the robot surface, but more rapid decrease with distance.

In summary, the speeds and sizes considered here are not likely to immediately damage nearby cells. Less disruptive methods have higher safety margin, especially when used in highly viscous fluids. Low-disruption methods may be important for long-term use of the robots to reduce the possibility of undesired chronic response to shear forces [25]. For slow movement within cells, where the robot will pass internal structures

at less than micron distances, the rapid decrease in disturbance with distance from the oscillating surface method could be particularly useful. Conversely, robots could deliberately exert forces on cells by activating propulsion while blocked by the cell membranes. These forces could achieve pressures high enough to affect the cells, thereby imposing microscopically precise patterns of forces throughout tissues.

In addition to their effect on nearby cells, robot motion will affect other nearby robots through hydrodynamic interactions [32, 46]. Locomotion methods that reduce these interactions simplify navigation control for robots moving near each other. One example is robots working together to build structures, especially with short time constraints and hence relatively rapid movements, such as forming clots in response to ruptured blood vessels [24]. Another example is nearby communicating robots combining measurements to determine spatial gradients more accurately and more rapidly than individual robots [16]. For instance, one robot collecting chemical measurements from a particular location would benefit from minimal disturbance to the fluid from other passing robots. For successive robots measuring spatial gradients of chemicals from nearby cells, reducing fluid disturbance each time a robot passes also reduces changes to the chemical gradient and hence reduces measurement noise. Thus less disruptive propulsion methods improve spatial gradient measurements repeated by multiple robots.

6 Robot Shape

For simplicity, the above discussion focused on spherical robots. This section describes locomotion design constraints related to robot shape [17, 23].

6.1 Geometric Constraints on Robot Shape

Elongated shapes can have high hydrodynamic efficiency. Nevertheless, design goals other than locomotion could significantly constrain the robot shape. In particular, geometric constraints include:

- volume

The robot volume must encompass all required internal components, such as power generation, control and chemical storage, e.g., for drug delivery.

- surface area

The robot surface must be large enough for all components that interact directly with the robot's environment. These may include surface propulsion, sensors and pumps that collect chemicals from the surrounding fluid and components for forming mechanical connections with other robots.

- minimum diameter

The minimum diameter determines the smallest gaps the robot could pass through, or the amount adjacent cells must be displaced when moving between them.

- maximum diameter

The maximum diameter determines the minimum size vessels device can pass through if passing at random orientations or as a safety constraint if orientation control fails. The largest diameter also affects detection of chemical gradients using sensors located on opposite ends of the robot [17].

- minimum radius of curvature

The minimum radius of curvature, i.e., how pointy the shape is, affects safety. A small radius means the robot has sharp ends that could puncture cells by applying the full force of locomotion over a tiny area.

The minimum radius of curvature also constrains the volume available for internal components next to the surface, e.g., a sensor at each end of the maximum diameter to detect chemical gradients [17].

Pointy ends give rise to large diffusive fluxes, which could overwhelm sensors or pumps even though those components readily handle the average flux over the entire surface. Conversely, pointy ends could

be useful enhancements of diffusion of low-concentration chemicals to the robot as an alternative to using many sensors spread over the full surface of a less pointy shape.

These geometric constraints interact to restrict the allowable range of shapes, with some constraints dominant for near-spherical shapes while others, e.g., radius of curvature, dominating extremely elongated shapes.

6.2 Example: Prolate Spheroids

While most shapes are not amenable to analytic solutions, the results discussed above for spheres extend to spheroids and general ellipsoids [17,32]. In particular, extending Eq. 3 and 5 to spheroids shows that a prolate spheroid (Fig. 11) has larger hydrodynamic efficiency and less disturbance to the fluid than a sphere of the same volume [50]. The small-amplitude analysis discussed above extends to spheroids and non-axisymmetric surface motions such as helical surface waves [20]. These geometries allow examining the effect of robot shape on locomotion.

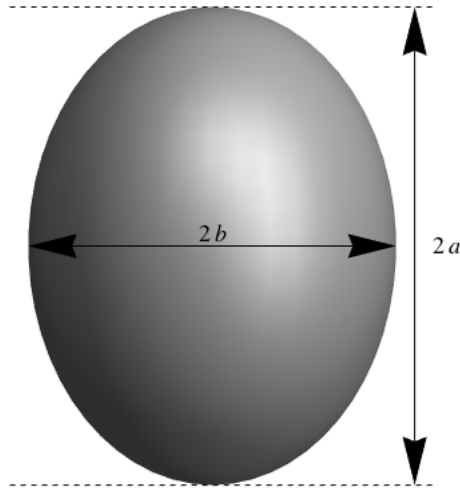


Figure 11: Prolate spheroid with semi-major and semi-minor axes of length a and b , respectively, with $a > b$. When $a = b$, the shape is a sphere with radius a .

Comparing different shapes requires selecting appropriate geometric constraints. A common choice is to compare shapes with constant *total* volume [17]. For robots, a more realistic choice accounts for the constraints required by the robot task, not just for locomotion itself. That is, locomotion gets the robot to suitable locations, but it needs other components to perform its task at the location. For example, the robot could need to carry a certain volume of drug to deliver to a cell identified by sensors on its surface. Thus as an example of design trade-offs related to shape, consider a task requiring the robot move at speed U and have volume and surface area available for non-propulsion components of at least $V_{\text{np}}^{\text{min}}$ and $S_{\text{np}}^{\text{min}}$, respectively. Propulsion components not only use some of the robot surface, but also occupy some volume of the robot near the surface. Thus both the total volume and surface area could vary with the shape.

As a specific case, we consider tangential motion on an equatorial band covering half the sphere's surface, as discussed with Table 2, and implemented with treadmills with sizes given in Section 3.2. The treadmill housing extends a distance equal to about the bearing diameter $2r = 100 \text{ nm}$ below the robot surface. Thus propulsion covering surface area S_p also uses volume $2rS_p$ within the robot. In this example, the sphere with radius $a_{\text{sphere}} = 1 \mu\text{m}$ has half its surface area available for non-propulsion components. Supposing this is the smallest sphere able to perform the task from both volume and surface area requirements, the geometry constraints are

$$V_{\text{np}} \geq V_{\text{np}}^{\text{min}} = \frac{4\pi}{3} a_{\text{sphere}}^3 - 2r(2\pi a_{\text{sphere}}^2) = 3.56 \mu\text{m}^3 \quad (14)$$

$$S_{\text{np}} \geq S_{\text{np}}^{\text{min}} = 2\pi a_{\text{sphere}}^2 = 6.28 \mu\text{m}^2 \quad (15)$$

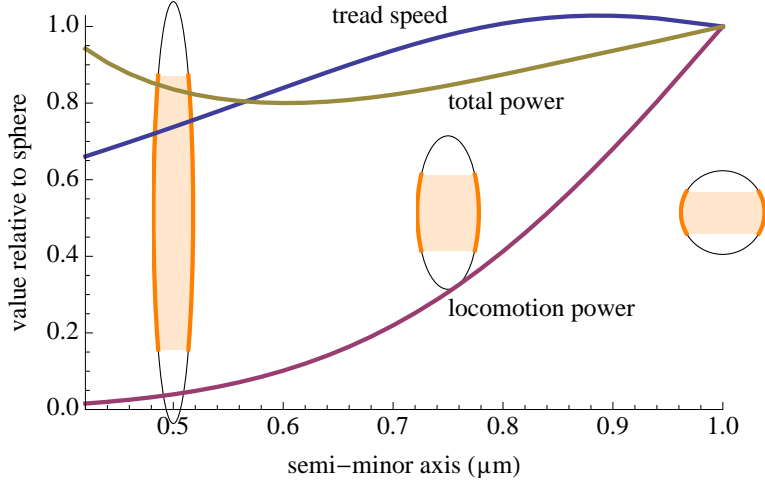


Figure 12: Tread speed, locomotion power and total power, relative to values for a sphere, as a function of robot shape for the LOW scenario. Locomotion is from steady tangential motion on a band around the equator, as discussed in Section 3. Robots move at the same speed ($U = 100 \mu\text{m/s}$), and have the same volume and surface area available for non-propulsion components. The ovals are cross sections of the robots corresponding to three values of the semi-minor axis indicated on the horizontal axis. The bands around the equatorial regions indicate the surface area devoted to propulsion.

An additional geometric constraint is that the robot is wide enough over the equatorial band to fit the tread housings. The cases considered here satisfy this constraint for $b \gtrsim 0.3 \mu\text{m}$.

Elongated shapes have more surface area for a given volume than a sphere. Thus a reasonable design comparison is among shapes of the smallest possible volume and total power dissipation. The total power is the sum of the external dissipation P_{propel} (“locomotion power”) and the upper bound estimate for internal dissipation P_{internal} for the treadmill implementation described in Section 3.2. This choice gives $V_{\text{np}} = V_{\text{np}}^{\text{min}}$ and $S_{\text{np}} = S_{\text{np}}^{\text{min}}$, i.e., using all additional surface area from an elongated shape for propulsion. One reason for this choice is the increasing hydrodynamic efficiency with size of the band, analogous to the case for spheres seen in Table 2. Internal power dissipation is a more significant factor. More propulsion components increase the sliding surface area but also allow the treads to operate more slowly for the required locomotion speed U . In this case, the decrease in tread speed more than offsets the increase in sliding area, leading to minimum power use when the tread covers as large an area as allowed by Eq. 15.

Fig. 12 shows the performance of various shapes with these constraints. The tread speed is relatively insensitive to shape, but hydrodynamic efficiency is significantly larger for elongated robots, resulting in lower locomotion power [50]. On the other hand, total power increases for sufficiently elongated shapes due to the increasing internal dissipation.

The increase in total power use for narrow robots illustrates the importance of including internal power dissipation in evaluating designs: the common focus solely on hydrodynamic efficiency would, in this case, misleadingly suggest using highly elongated “needle” shapes, at least as far as power use is concerned.

By contrast, in the HIGH scenario, internal drag is negligible. The 100 times slower speed gives 10^4 times less internal friction, while the locomotion power is the same due to the higher viscosity.

7 Brownian Motion

Microscopic robots not only face challenges of moving in viscous fluids, but also Brownian motion, which randomly changes both the robot’s location and orientation. An example scenario is a group of robots released together with specified initial orientations. These directions could be uniformly distributed so the robots examine all nearby cells for diagnosis. Alternatively, the robots may be aimed in the same direction, e.g., to

scenario		LOW	HIGH
translation diffusion coefficient	D	$2 \times 10^{-13} \text{ m}^2/\text{s}$	$2 \times 10^{-17} \text{ m}^2/\text{s}$
rms displacement after $d = 100 \mu\text{m}$	$\sqrt{6Dd/U}$	$1 \mu\text{m}$	$0.1 \mu\text{m}$
time constant for orientation loss	τ	3 s	8 hr
travel distance during orientation time	$U\tau$	$300 \mu\text{m}$	30 mm
motile diffusion coefficient	D_m	$10^{-8} \text{ m}^2/\text{s}$	$10^{-8} \text{ m}^2/\text{s}$

Table 7: Effects of Brownian motion on a sphere with radius of $1 \mu\text{m}$ for the scenarios of Table 1. For comparison, small molecules in water at body temperature have $D \approx 10^{-9} \text{ m}^2/\text{s}$.

carry a large volume of drug to one specific cell.

The simplest navigation is dead reckoning: the robots continue in their initial directions until they reach their target locations. Brownian motion limits the accuracy of this approach, thereby requiring more complex navigation methods. One of such method is using reference signals from nearby implanted navigation nodes [23], which requires sensors and control computations. Another approach is stabilizing orientation with a gyroscope, using a substantial fraction of a micron-size robot’s volume [23]. An alternative to more complex navigation for individual robots is to use a larger number of simpler robots so that enough robots reach the intended locations to complete the task. Extending this approach, traveling in swarms in which each robot adjusts its direction based on the observed orientation of its neighbors [7]. Such adjustments reduce the effect of Brownian motion: the average direction of swarm will change more slowly than the direction of an individual robot.

While these are possible approaches to navigation, identifying cases where dead reckoning is sufficient will allow using simpler robots. Specifically, the diffusion constant of a sphere of radius a in fluid with viscosity η at temperature T is

$$D = \frac{k_B T}{6\pi a \eta} \quad (16)$$

where k_B is the Boltzmann constant. The change in position after time t is of order $\sqrt{6Dt}$. Brownian motion also affects robot orientation, specifically changing orientation of an axis of a sphere with time constant [17]

$$\tau = \frac{4a^3 \pi \eta}{k_B T} \quad (17)$$

Table 7 gives these values for the two scenarios, and the typical displacement during the time a robot moves $100 \mu\text{m}$. The orientation time is much longer than needed for the robot to actively change its orientation, as described with Table 3. Thus these effects of Brownian motion are fairly minor for motion over the times and distances of the scenarios of Table 1.

For self-propelled objects, a more significant effect is change in robot orientation as the robot moves. Over times large compared to τ , the random orientation changes lead to diffusive motion of self-propelled objects characterized by the motile diffusion coefficient $D_m = \tau U^2/3$ where U is the robot’s speed [5, 17]. Table 7 shows this diffusion is much more rapid than that due to translational diffusion. Maintaining direction over such times will require more complex navigation methods.

On the other hand, for times comparable or shorter than the orientation loss time τ , locomotion remains predominantly in the original direction. This is the relevant case for motion over a few cell diameters, $100 \mu\text{m}$ or so, or in very viscous fluids. In this regime, the main effect of orientation loss is a limit on how far a robot can accurately navigate by dead reckoning. The root-mean-square (rms) angle change is $\alpha_{\text{rms}} = \sqrt{t/\tau}$ in time t , during which the robot moves distance Ut . If the robot must reliably move distance d with rms angle change at most α_{rms} , then it must move at least as fast as $U = d/t = d/(\tau \alpha_{\text{rms}}^2)$. One consequence of this constraint is an increase in energy required for smaller τ : power dissipation is proportional to U^2 while the time for the motion is d/U , giving energy use proportional to U . Thus expending more energy on locomotion extends the useful range of dead reckoning.

Robot geometry significantly affects Brownian motion. For instance, orientation time (Eq. 17) increases rapidly with size, so even somewhat larger robots can more effectively use dead reckoning. Robot shape is also important. Fig. 13 shows an example with the same geometry constraints as in Fig. 12 for an allowed

change in orientation of $\alpha_{\text{rms}} = 20^\circ$ rms over a distance $d = 20 \mu\text{m}$. This gives a location error of order $d \sin \alpha_{\text{rms}} = 7 \mu\text{m}$, i.e., less than a typical cell diameter. Elongated robots maintain direction for a longer time, thereby allowing them to meet the navigation requirement with slower motion. Elongated robots also dissipate less energy, both internal and external, during the motion: the smaller dissipation of lower locomotion speeds more than compensates for the increased time to reach the location. Thus choices of locomotion speed and robot shape can extend the applicability of dead reckoning navigation.

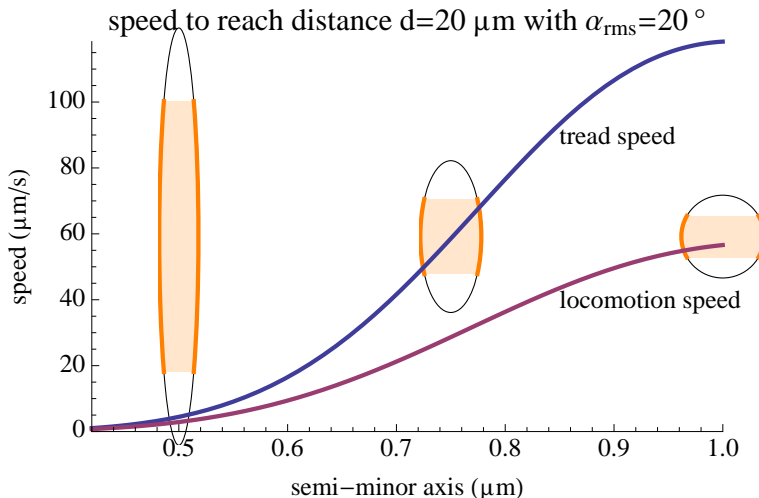


Figure 13: Locomotion speed required for dead reckoning navigation in fluid with the viscosity of the LOW scenario, over a distance of $20 \mu\text{m}$ for robots shaped as prolate spheroids with the same volume and surface area used for non-propulsion components. The ovals are cross sections of the robots corresponding to three values of the semi-major axis indicated on the horizontal axis. The bands around the equatorial regions indicate the surface area devoted to propulsion.

8 Choice of Propulsion Method

This paper examines two propulsion mechanisms: steady tangential surface motion and periodic surface oscillations. This section discusses their relative merits.

8.1 Steady Tangential Motion

Steady tangential surface motion can move the robot with large hydrodynamic efficiency and produce relatively high thrust and speeds compared to small amplitude oscillations.

Tangential motion does not change the robot's shape. This could be useful when operating in regions with rigid walls where changing shape, especially change in volume, could result in large pressure changes in the surrounding fluid.

Treadmills could move the robot over solid surfaces [23] in addition to movement in fluids, thereby providing operational flexibility.

Steady tangential motion has more implementation uncertainty than surface oscillations. One example of this uncertainty is avoiding leaks of fluid into the robot where the moving surface enters the robot. There is also the question of fatigue in the materials after long operation, which affects the reliability of the locomotion mechanism. On the other hand, we already have extensive experience with small-amplitude surface motions produced by piezoelectric materials, though generally at larger scales than considered here.

In summary, propulsion by steady surface motion is especially useful for tasks that 1) require fast or efficient locomotion, especially in highly viscous fluids, 2) operate in confined regions or alternate between

moving in fluid and on solid surfaces, and 3) have significant available surface area to devote to propulsion.

8.2 Surface Oscillations

Forces applied within the robot can produce surface oscillations. Thus other components, such as sensors, can use the same surface area that provides motion (provided they function in spite of the oscillations). Since oscillation amplitude is largest near the equator, less flexible surface components could be placed near the poles.

At higher frequencies, oscillations can perform functions other than locomotion, e.g., sensing, navigation and communication [23, 37]. Thus an implementation that can operate at a wide range of frequencies can provide several functions for the robot.

With surface oscillations, a spherical robot can alter direction simply by changing the oscillation pattern. This contrasts with steady motion implemented by treadmills or wheels in fixed orientation on the surface: such propulsion requires a separate step to rotate the robot.

Small-amplitude surface waves are likely easier to implement than methods requiring moving parts of the robot over long distances. In particular, oscillations avoid the need for watertight breaks in the surface.

Small-amplitude surface waves only slightly disturb surrounding fluid beyond a narrow boundary layer around the robot. Robots may need to enter and move through the interior of cells [23] where propulsion methods with minimal disturbance may be particularly important to avoid damage. Such intracellular motion would be autonomous extensions of inserting probes into cells, which do not appear to damage the cells even after several days [30, 83].

In summary, propulsion by small surface oscillations is especially useful for task that 1) require most of the surface area for other uses and hence have little area available for separate propulsion components (without increasing the robot size), and 2) do not require fast or efficient locomotion.

8.3 Example of Design Trade-offs

Having presented two propulsion methods for microscopic robots, this section illustrates the choice among these methods in the context of conservative design constraints. Such constraints correspond to large safety margins in designs, which are particularly appropriate for early use of nanorobots whose capabilities may be limited and which operate with significant uncertainties in the physical properties of their microenvironments and how cells respond to their motion.

As a specific example, we consider the following design constraints. First, we allow up to 1 pW for power dissipation, leaving most of the robot's available power (i.e., tens of picowatts) for other tasks. For shear stress, we use the conservative limit from Section 5 of 1 Pa at a distance of 1 μm from the robot. We compute this shear force based on the gradient in fluid velocity near the robot surface shown in Fig. 10. We suppose robots use dead reckoning for navigation, with the example discussed in Section 7 as the limiting constraint.

Fig. 14 illustrates design trade-offs from these constraints. The speed and viscosity values in the diagram cover much of the range relevant for *in vivo* operation. The locomotion speeds range from 1 $\mu\text{m}/\text{s}$, allowing moving a few cell diameters in a minute, to 1 cm/s, a conservative upper limit to avoid damage to cells from collisions with the robots [23]. The range of viscosities includes most biological fluids [23], with water and blood plasma at the left, cell cytoplasm on the right.

The diagram shows power and shear stress limit operation in high viscosity fluids or at high speeds³. Tangential motion is more efficient than surface oscillations, but also has larger shear stresses. The effect of Brownian motion on navigation is only significant for slower motion in low viscosity fluids. Over most of the diagram, power limits arise mainly from external fluid drag. Only at the upper left, i.e., high speeds in less viscous fluids, do internal losses contribute noticeably.

³ At the upper left of the diagram, the Womersley number is close to 1 so the quasi-static approximation in Section 4 is less accurate [46]. Corrections are not significant for this example since this portion of the diagram is outside the feasible operation range.

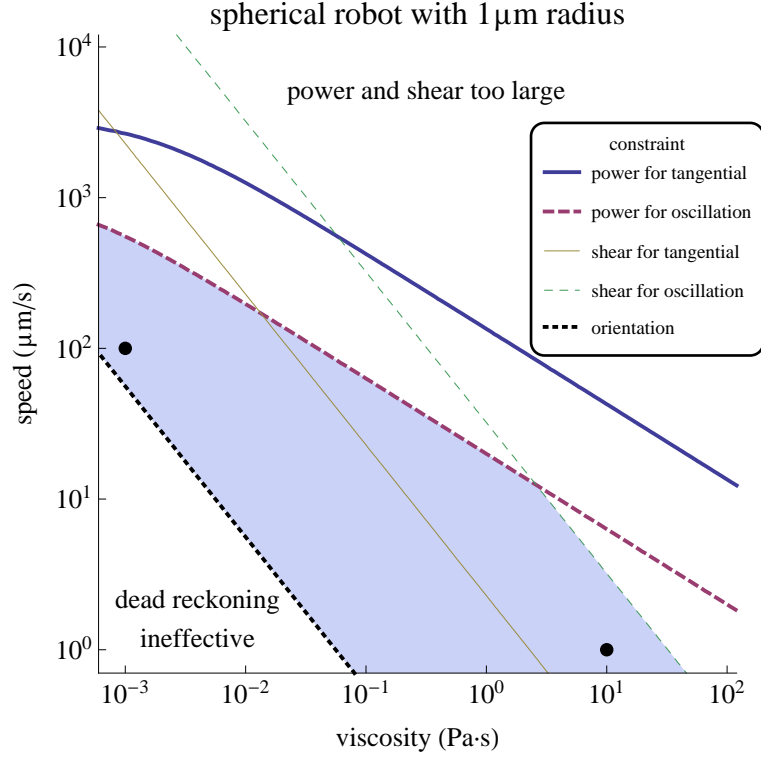


Figure 14: Performance constraints for a spherical robot using either tangential motion on an equatorial band covering half the surface (solid) or surface oscillations (dashed). The axes use logarithmic scales. The lines indicate constraints: power of 1 pW, shear stress $1 \mu\text{m}$ from the robot surface of 1 Pa and Brownian motion giving $\alpha_{\text{rms}} = 20^\circ$ over a distance $d = 20 \mu\text{m}$. Surface oscillations satisfy all the constraints in the shaded area. The black dots indicate the scenarios of Table 1.

Consequences of these limits depend on nanorobot task and range of environments they operate in. For instance, general purpose robots will operate at a wide range of speeds in fluids of various viscosities. Propulsion by surface oscillations provide a range of possibilities satisfying these constraints (shaded area in Fig. 14). On the other hand, specialized robots could be optimized for a limited range of speeds and fluid viscosity. One such example is robots that move rapidly in small blood vessels, especially to move upstream against the flow, requiring speeds around $10^3 \mu\text{m/s}$ but only in low viscosity fluids. Another example is a robot needing to actively move only a few cell diameters away from capillaries over the course of several minutes, so speeds of $1 \mu\text{m/s}$ or less are sufficient but the fluid may be highly viscous.

Fig. 14 also shows that tasks requiring higher performance (e.g., high speed in viscous fluids) will violate some of the constraints. For example, the robot could devote a more substantial fraction of its power to locomotion, thereby having less capability for other tasks, e.g., communication or on-board computation to evaluate sensor readings. Another example is moving slowly in low viscosity fluids which requires more complicated navigation than dead reckoning.

Elongated robot shapes improve power efficiency and reduce the effect of Brownian motion, so are useful designs provided they satisfy geometric constraints, which are not included in Fig. 14. This discussion also does not include the maximum thrust force the robots could produce.

9 Conclusion

This paper evaluated locomotion for microscopic robots in biological fluids. Two appealing designs are steady tangential surface motion and periodic surface oscillations. Both methods give speed and maneuverability

sufficient for a variety of biomedical research, diagnostic and treatment applications. Moreover, these designs allow devoting a significant fraction of the robot surface to other, non-propulsion devices, such as sensors. These locomotion methods produce relatively little disturbance of the surrounding fluid and avoid potential damage or tangling from using extended structures such as flagella. These features make locomotion compatible with other design goals, such as sensing, drug delivery and safety. Furthermore, the machines will likely have more than enough power for these modes of locomotion.

Estimating internal power dissipation is challenging, both for microorganisms and robots, which leads most analyses of locomotion to focus on hydrodynamic efficiency as the primary power criterion. For microscopic robots made of precise, stiff materials, sliding friction dominates internal power dissipation, which allows rough estimates of internal dissipation. Including these estimates with the power evaluation emphasizes different designs than a focus on hydrodynamic efficiency alone would suggest. In particular, when considering robot shape, internal dissipation limits the benefit of increasingly elongated shapes.

A robot could have multiple locomotion modes for redundancy and providing different trade-offs for operation in different environments. For instance, a robot could use treadmills for high-efficiency in fluids far from cells where damage to membranes is not an issue, and oscillating surfaces for locomotion near or within cells.

The implementations discussed in this paper focus on the surface components, which directly interact with the fluid, i.e., treadmills, wheels and oscillating surfaces. Robots need additional components to produce and control these surface motions. Thus a question for future study is designing and evaluating internal components. One important property of these components is their energy dissipation. Another important property is the failure rates of these mechanisms [14]. These rates determine long-term reliability [75] of the locomotion and hence the redundancy required to have high confidence that robots can complete their tasks.

Reliable locomotion of *in vivo* nanorobots require controls [28] suited to the millisecond time and micron space scales of robot motion. These controls include both individual robot behavior [3, 54] and coordinated behaviors of multiple nearby robots (e.g., swarms) due to hydrodynamic interactions [33, 41, 44, 46, 48, 67]. Sensors for the status of propulsion components can help ensure safe operation and allow closed-loop locomotion control. Such sensors include measuring the speed of propulsion components on the robot surface and forces on those components [23]. Unusual speeds or forces could indicate component failure or that the robot is stuck. The controller could respond to avoid damage to the robot or its surroundings by either fixing the problem (e.g., deactivating out-of-spec propulsion components) or, as a last resort, placing the robot in a passive “safe mode”.

A potential problem with rapidly moving components is whether they make the robot as a whole resonate, thereby building up large and potentially destructive oscillations. As an estimate of relevant resonant frequencies, consider a piston with stiffness $k_s \sim 25$ N/m and mass $m \sim 4 \times 10^{-15}$ kg for a cubic micron nanorobot as typical of proposed materials for microscopic robots. The lowest resonant frequency is $f_{\text{res}} \sim 10$ MHz [23]. This is much larger than the propulsion frequencies we consider, so resonances from locomotion in micron-scale robots are unlikely.

Fabrication of complex structures with stiff materials may create other propulsion methods, including jets with the possibility of arbitrarily small disturbance to the surrounding fluid [71], propellers [80], acoustic streaming [19, 52], and moving extended structures such as flagella and cilia. For example, flagella consisting of stiff, telescoping rods could reduce drag, compared to similar microorganism propulsion, by retracting the rod during the recovery stroke, and simultaneously reduce the opportunities for tangling or damaging nearby cells.

This paper focussed on steady locomotion in fluid with fixed properties on the scale of the robots. Important extensions beyond this setting include motion in biological tissues with significant viscoelasticity [23, 48], and motion through small spaces, e.g., through narrow channels within bone, where boundary effects are significant [32, 33, 46, 67]. Robots may be able to exploit these effects, such as by using deformable boundaries to improve locomotion performance [76]. Another extension is moving in bursts, which could use more power than available for steady motion, hence achieving higher speeds or forces. This could be especially useful for operating in very viscous fluids.

Biological tissues change at both large and small space and time scales in response to environmental signals. Feedback control can allow robots to compensate for such changes. Moreover, robots could initiate such

changes through active signaling to alter the robot's environment as it moves. For example, the propulsion mechanism can apply mechanical forces on individual nearby cells. Alternatively, the robot could release chemical signals from onboard storage tanks. A potential application for such signals is moving between cells forming the boundary of tissues, such as blood vessel walls, without damaging cells, by signaling them to change adhesive forces, similar to signals used by white blood cells to exit vessels [2, 51].

Robots could act together to produce larger mechanical forces or chemical concentrations than a single robot. Such coordinated activity includes creating patterns of forces on cells over extended periods of time, which can change the cell arrangement and function [12].

Future evaluation of these questions will clarify locomotion design trade-offs for microscopic robots. Fabrication of such robots involve significant technological challenges. Prior to the feasibility of such fabrication, theoretical studies, such as presented in this paper, quantify likely nanorobot capabilities and their suitability for various applications. In particular, the evaluation of locomotion options provides guidelines for designs and indicates alternative implementations providing the same capabilities. This variety of options increases confidence that microscopic robots will have at least some feasible methods for locomotion.

References

- [1] Jake J. Abbott et al. How should microrobots swim? *Intl. J. of Robotics Research*, 28:1434–1447, 2009.
- [2] Ann Ager. Inflammation: Border crossings. *Nature*, 421:703–705, 2003.
- [3] F. Alouges et al. Numerical strategies for stroke optimization of axisymmetric microswimmers. *Mathematical Models and Methods in Applied Sciences*, 21:361–387, 2011.
- [4] Bahareh Behkam and Metin Sitti. Bacterial flagella-based propulsion and on/off motion control of microscale objects. *Applied Physics Letters*, 90:023902, 2007.
- [5] Howard C. Berg. *Random Walks in Biology*. Princeton Univ. Press, 2nd edition, 1993.
- [6] J. R. Blake. A spherical envelope approach to ciliary propulsion. *J. of Fluid Mechanics*, 46:199–208, 1971.
- [7] Eric Bonabeau, Marco Dorigo, and Guy Theraulaz. *Swarm Intelligence: From Natural to Artificial Systems*. Oxford University Press, Oxford, 1999.
- [8] C. Brennen. An oscillating-boundary-layer theory for ciliary propulsion. *J. of Fluid Mechanics*, 65:799–824, 1974.
- [9] Christopher Brennen and Howard Winet. Fluid mechanics of propulsion by cilia and flagella. *Annual Review of Fluid Mechanics*, 9:339–398, 1977.
- [10] Mei Lin Chan et al. Low friction liquid bearing mems micromotor. In *Proc. of 24th IEEE Intl. Conf. on Micro Electro Mechanical Systems (MEMS)*, pages 1237–1240, 2011.
- [11] Benjamin P. C. Chen et al. DNA microarray analysis of gene expression in endothelial cells in response to 24-h shear stress. *Physiological Genomics*, 7:55–63, 2001.
- [12] P. F. Davies. Flow-mediated endothelial mechanotransduction. *Physiological Reviews*, 75:519–560, 1995.
- [13] Dennis E. Discher, Paul Janmey, and Yu-li Wang. Tissue cells feel and respond to the stiffness of their substrate. *Science*, 310:1139–1143, 2005.
- [14] K. Eric Drexler. *Nanosystems: Molecular Machinery, Manufacturing, and Computation*. John Wiley, NY, 1992.
- [15] Remi Dreyfus et al. Microscopic artificial swimmers. *Nature*, 437:862–865, 2005.

- [16] David B. Dusenbery. Spatial sensing of stimulus gradients can be superior to temporal sensing for free-swimming bacteria. *Biophysical Journal*, 74:2272–2277, 1998.
- [17] David B. Dusenbery. *Living at Micro Scale: The Unexpected Physics of Being Small*. Harvard Univ. Press, Cambridge, MA, 2009.
- [18] K. M. Ehlers, A. D. T. Samuel, H. C. Berg, and R. Montgomery. Do cyanobacteria swim using traveling surface waves? *Proc. of the Natl. Acad. of Sciences USA*, 93:8340–8343, 1996.
- [19] Kurt M. Ehlers and Jair Koiller. Could cell membranes produce acoustic streaming? making the case for *Synechococcus* self-propulsion. *Mathematical and Computer Modelling*, 53:1489–1504, 2011.
- [20] Kurt M. Ehlers and Jair Koiller. Micro-swimming without flagella: Propulsion by internal structures. *Regular and Chaotic Dynamics*, 16:623–652, 2011.
- [21] Alexander L. Fetter and John Dirk Walecka. *Theoretical Mechanics of Particles and Continua*. McGraw-Hill, NY, 1980.
- [22] Robert A. Freitas Jr. Exploratory design in medical nanotechnology: A mechanical artificial red cell. *Artificial Cells, Blood Substitutes and Immobilization Biotechnology*, 26:411–430, 1998.
- [23] Robert A. Freitas Jr. *Nanomedicine*, volume I: Basic Capabilities. Landes Bioscience, Georgetown, TX, 1999. Available at www.nanomedicine.com/NMI.htm.
- [24] Robert A. Freitas Jr. Clottocytes: Artificial mechanical platelets. IMM Report 18: Nanomedicine, Institute for Molecular Manufacturing, Palo Alto, CA, 2000.
- [25] Robert A. Freitas Jr. *Nanomedicine*, volume IIA: Biocompatibility. Landes Bioscience, Georgetown, TX, 2003. Available at www.nanomedicine.com/NMIIA.htm.
- [26] Robert A. Freitas Jr. Pharmacytes: An ideal vehicle for targeted drug delivery. *Journal of Nanoscience and Nanotechnology*, 6:2769–2775, 2006.
- [27] Robert A. Freitas Jr. The ideal gene delivery vector: Chromalloytes, cell repair nanorobots for chromosome replacement therapy. *J. of Evolution and Technology*, 16:1–97, 2007.
- [28] Robert A. Freitas Jr. Computational tasks in medical nanorobotics. In M.M. Eshaghian-Wilner, editor, *Bio-inspired and Nano-scale Integrated Computing*, chapter 15, pages 391–428. John Wiley, NY, 2009.
- [29] Y. C. Fung. *Biomechanics: Circulation*. Springer, NY, 2nd edition, 1997.
- [30] R. Gao et al. Outside looking in: Nanotube transistor intracellular sensors. *Nano Letters*, 12:3329–3333, 2012.
- [31] Jeffrey S. Guasto, Roberto Rusconi, and Roman Stocker. Fluid mechanics of planktonic microorganisms. *Annual Reviews of Fluid Mechanics*, 44:373–400, 2012.
- [32] John Happel and Howard Brenner. *Low Reynolds number hydrodynamics*. Kluwer, The Hague, 2nd edition, 1983.
- [33] Juan P. Hernandez-Ortiz, Christopher G. Stoltz, and Michael D. Graham. Transport and collective dynamics in suspensions of confined swimming particles. *Physical Review Letters*, 95:204501, 2005.
- [34] Ciaran Hill, Antonio Amodeo, Jean V. Joseph, and Hitendra R. H. Patel. Nano- and microrobotics: how far is the reality? *Expert Review of Anticancer Therapy*, 8:1891–1897, 2008.
- [35] Tad Hogg. Coordinating microscopic robots in viscous fluids. *Autonomous Agents and Multi-Agent Systems*, 14(3):271–305, 2007.
- [36] Tad Hogg and Robert A. Freitas Jr. Chemical power for microscopic robots in capillaries. *Nanomedicine: Nanotechnology, Biology, and Medicine*, 6:298–317, 2010.

- [37] Tad Hogg and Robert A. Freitas Jr. Acoustic communication for medical nanorobots. *Nano Communication Networks*, 3:83–102, 2012.
- [38] Tad Hogg and Philip J. Kuekes. Mobile microscopic sensors for high-resolution in vivo diagnostics. *Nanomedicine: Nanotechnology, Biology, and Medicine*, 2:239–247, 2006.
- [39] Tad Hogg and David W. Sretavan. Controlling tiny multi-scale robots for nerve repair. In M. Veloso and S. Kambhampati, editors, *Proc. of the 20th Natl. Conf. on Artificial Intelligence (AAAI2005)*, pages 1286–1291. AAAI Press, 2005.
- [40] Hayden Huang et al. Cell mechanics and mechanotransduction: pathways, probes, and physiology. *American J. of Physiology: Cell Physiology*, 287:C1–C11, 2004.
- [41] Takuji Ishikawa and T. J. Pedley. Coherent structures in monolayers of swimming particles. *Physical Review Letters*, 100:088103, 2008.
- [42] K. Ishiyama, M. Sendoh, and K. I. Arai. Magnetic micromachines for medical applications. *J. of Magnetism and Magnetic Materials*, 242-245:41–46, 2002.
- [43] Theodore L. Jahn and John J. Votta. Locomotion of protozoa. *Annual Review of Fluid Mechanics*, 4:93–116, 1972.
- [44] Alex Kanevsky, Michael J. Shelley, and Anna-Karin Tornberg. Modeling simple locomotors in Stokes flow. *J. of Computational Physics*, 229:958–977, 2010.
- [45] Stuart R. Keller and Theodore Y. Wu. A porous prolate-spheroidal model for ciliated micro-organisms. *J. of Fluid Mechanics*, 80:259–278, 1977.
- [46] S. Kim and S. J. Karrila. *Microhydrodynamics*. Dover, 2005.
- [47] Jacqueline Krim. Surface science and the atomic-scale origins of friction. *Surface Science*, 500:741–758, 2002.
- [48] Eric Lauga and Thomas R. Powers. The hydrodynamics of swimming microorganisms. *Reports on Progress in Physics*, 72:096601, 2009.
- [49] Changgu Lee et al. Measurement of the elastic properties and intrinsic strength of monolayer graphene. *Science*, 321:385–388, 2008.
- [50] A. M. Leshansky et al. A frictionless microswimmer. *New Journal of Physics*, 9:145, 2007.
- [51] Klaus Ley et al. Getting to the site of inflammation: the leukocyte adhesion cascade updated. *Nature Reviews Immunology*, 7:678–689, 2007.
- [52] James Lighthill. Acoustic streaming. *J. of Sound and Vibration*, 61:391–418, 1978.
- [53] M. J. Lighthill. On the squirming motion of nearly spherical deformable bodies through liquids at very small reynolds numbers. *Communications on Pure and Applied Mathematics*, 5:109–118, 1952.
- [54] J. Loheac et al. Controllability and time optimal control for low Reynolds numbers swimmers. *Acta Applicandae Mathematicae*, 123:175–200, 2013.
- [55] S. Martel et al. Automatic navigation of an untethered device in the artery of a living animal using a conventional clinical magnetic resonance imaging system. *Applied Physics Letters*, 90:114105, 2007.
- [56] Sylvain Martel. The coming invasion of the medical nanorobots. *Nanotechnology Perceptions*, 3:165–173, 2007.
- [57] Sylvain Martel et al. Flagellated bacterial nanorobots for medical interventions in the human body. In D. Meldrum and O. Khatib, editors, *Proc. of 2nd IEEE Conf. on Biomedical Robotics and Biomechanics*, pages 264–269, 2008.

- [58] Alex V. Mezheritsky. Elastic, dielectric, and piezoelectric losses in piezoceramics: how it works all together. *IEEE Trans. on Ultrasonics, Ferroelectrics and Frequency Control*, 51:695–707, 2004.
- [59] Sebastien Michelin and Eric Lauga. Efficiency optimization and symmetry-breaking in a model of ciliary locomotion. *Fluid Dynamics*, 22:111901, 2010.
- [60] Philip Nelson. *Biological Physics: Energy, Information, Life*. W. H. Freeman, NY, 2008.
- [61] N. Olamaei, F. Cheriet, G. Beaudoin, and S. Martel. MRI visualization of a single $15\mu\text{m}$ navigable imaging agent and future microrobot. In *Proc. of the 2010 Conf. on Engineering in Medicine and Biology Society*, pages 4355–4358. IEEE, 2010.
- [62] Frank W. J. Oliver et al., editors. *NIST Handbook of Mathematical Functions*. Cambridge Univ. Press, 2010.
- [63] Mitchell T. Ong and Evan J. Reed. Engineered piezoelectricity in graphene. *ACS Nano*, 6:1387–1394, 2012.
- [64] Natan Osterman and Andrej Vilfan. Finding the ciliary beating pattern with optimal efficiency. *Proc. of the Natl. Acad. of Sci. USA*, 108:15727–15732, 2011.
- [65] T. G. Papaioannou and C. Stefanadis. Vascular wall shear stress: Basic principles and methods. *Hellenic J. Cardiology*, 46:9–15, 2005.
- [66] Edward M. Purcell. Life at low Reynolds number. *American Journal of Physics*, 45:3–11, 1977.
- [67] Ingmar H. Riedel et al. A self-organized vortex array of hydrodynamically entrained sperm cells. *Science*, 309:300–303, 2005.
- [68] A. Shapere and F. Wilczek. Geometry of self-propulsion at low Reynolds number. *J. of Fluid Mechanics*, 198:557–585, 1989.
- [69] Alfred Shapere and Frank Wilczek. Efficiencies of self-propulsion at low Reynolds number. *J. of Fluid Mechanics*, 198:587–599, 1989.
- [70] Ricky K. Soong et al. Powering an inorganic nanodevice with a biomolecular motor. *Science*, 290:1555–1558, 2000.
- [71] Saverio E. Spagnolie and Eric Lauga. Jet propulsion without inertia. *Physics of Fluids*, 22:081902, 2012.
- [72] Todd M. Squires and Stephen R. Quake. Microfluidics: Fluid physics at the nanoliter scale. *Reviews of Modern Physics*, 77:977–1026, 2005.
- [73] H. A. Stone and A. Samuel. Propulsion of microorganisms by surface distortions. *Physical Review Letters*, 77:4102–4104, 1996.
- [74] P. Stone and M. Veloso. Multiagent systems: A survey from a machine learning perspective. submitted to *IEEE Transactions on Knowledge and Data Engineering*, June 1996.
- [75] Paul A. Tobias and David C. Trindade. *Applied Reliability*. Van Nostrand Reinhold, NY, 1986.
- [76] Renaud Trouilloud et al. Soft swimming: Exploiting deformable interfaces for low Reynolds number locomotion. *Physical Review Letters*, 101:048102, 2008.
- [77] Kenji Uchino. Piezoelectric ceramics. In S. Somiya et al., editors, *Handbook of Advanced Ceramics*, chapter 4.1, pages 107–160. Elsevier, 2003.
- [78] Andrea Vanossi et al. Modeling friction: From nanoscale to mesoscale. *Reviews of Modern Physics*, 85:529–552, 2013.

- [79] Viola Vogel and Michael Sheetz. Local force and geometry sensing regulate cell functions. *Nature Reviews: Molecular Cell Biology*, 7:265–275, 2006.
- [80] Boyang Wang and Petr Kral. Chemically tunable nanoscale propellers of liquids. *Physical Review Letters*, 98:266102, 2007.
- [81] Xudong Wang et al. Direct-current nanogenerator driven by ultrasonic waves. *Science*, 316:102–105, 2007.
- [82] Frank M. White. *Viscous Fluid Flow*. McGraw-Hill, 3rd edition, 2005.
- [83] Xi Xie et al. Nanostraw-electroporation system for highly efficient intracellular delivery and transfection. *ACS Nano*, 7:4351–4358, 2013.
- [84] Jiarui Yang et al. Observation of high-speed microscale superlubricity in graphite. *Physical Review Letters*, 110:255504, 2013.
- [85] J. Zhang et al. Large field-induced strains in a lead-free piezoelectric material. *Nature Nanotechnology*, 6:98–102, 2011.
- [86] Zhi-guo Zhou and Zhi-wen Liu. Biomimetic cilia based on MEMS technology. *J. of Bionic Engineering*, 5:358–365, 2008.